Applied Physics Letters

Iodine orbital moment and chromium anisotropy contributions to CrI_3 magnetism

Cite as: Appl. Phys. Lett. **117**, 022411 (2020); https://doi.org/10.1063/5.0012748
Submitted: 04 May 2020 . Accepted: 01 July 2020 . Published Online: 17 July 2020

Y. Choi, P. J. Ryan, D. Haskel, J. L. McChesney, G. Fabbris, M. A. McGuire, and J.-W. Kim

Applied Physics Letters ARTICLE scitation.org/journal/apl

Iodine orbital moment and chromium anisotropy contributions to CrI_3 magnetism

Cite as: Appl. Phys. Lett. **117**, 022411 (2020); doi: 10.1063/5.0012748
Submitted: 4 May 2020 · Accepted: 1 July 2020 ·
Published Online: 17 July 2020

Y. Choi,[1,a)] P. J. Ryan,[1] D. Haskel,[1] J. L. McChesney,[1] G. Fabbris,[1] M. A. McGuire,[2] and J.-W. Kim[1]

AFFILIATIONS

[1]Advanced Photon Source, Argonne National Laboratory, Argonne, Illinois 60439, USA
[2]Materials Science and Technology Division, Oak Ridge National Laboratory, Oak Ridge, Tennessee 37831, USA

[a)]Author to whom correspondence should be addressed: ychoi@anl.gov

ABSTRACT

The recent discovery of two-dimensional (2D) magnets, with a number of interesting magnetic properties, has drawn much interest due to their potential for future 2D spintronic device applications. CrI_3, a van der Waals magnet, exhibits two-dimensional ferromagnetism even in monolayer form, stabilized by strong magnetic anisotropy. Its interlayer magnetic ordering is coupled to structural layer stacking, implying that the charge density distribution mediating van der Waals interactions plays a key role in the magnetic interaction between the layers. Using polarization-dependent x-ray spectroscopy, we investigated the response of the electronic environment around Cr and I sites to structural changes of layer stacking order. The highly anisotropic nature of the Cr local environment is significantly enhanced and is accompanied by changes in the valence band, in the rhombohedral phase. Magnetic spectroscopy measurements reveal a sizable iodine orbital moment, indicating the iodine contribution to magnetic anisotropy. Our results uncover an important role for the extended nature of anisotropic Cr orbital states in dictating interlayer magnetic interactions and the iodine contribution to magnetic anisotropy.

The realization of two-dimensional magnetism in van der Waals material CrI_3, with readily cleavable atomically flat surfaces, makes it a potential spintronic material for magnetic tunneling junctions.[1–4] Although magnetic ordering is unstable in an isotropic Heisenberg two-dimensional system due to thermal fluctuations, a strong magnetic anisotropy can stabilize long-range magnetic order.[5] With a layered structure, CrI_3 exhibits ferromagnetism with a Curie temperature of 60 K due to sizable magnetic anisotropy along the out-of-plane direction. This anisotropy stabilizes long-range ferromagnetic order even in a single CrI_3 layer.[6] In bulk form, the crystal structure undergoes a structural transition near 210 K from rhombohedral to monoclinic on warming, which involves displacement of layer stacking.[7]

While ferromagnetism in CrI_3 is readily observable, the mechanisms behind ferromagnetism and magnetic anisotropy still remain an active research topic.[8–16] An experimentally observed value of $\sim 3\ \mu_B$/Cr suggests that the Cr^{3+} ions in CrI_3 should have $S = 3/2$ with a quenched orbital moment, indicating insignificant single ion anisotropy contribution from the Cr atoms. Indeed, x-ray magnetic circular dichroism (XMCD) at the Cr $L_{2,3}$ absorption edges, probing the Cr 3d states, has not shown any measurable orbital moment contribution,[15,17] and thus, this naturally leads to a postulation that the iodine ion is likely the main contributor to magnetic anisotropy. From previous studies, it is found that sizable spin–orbit coupling from I atoms and strong hybridization between the Cr 3d and I 5p states are linked to the stabilization of long-range ferromagnetic ordering and strong magnetic anisotropy.[8–15] Another interesting aspect of the CrI_3 material is an intricate coupling between layer stacking and exchange interactions. Modifying the layer stacking can tune the interlayer interaction between antiferromagnetic and ferromagnetic, with the monoclinic phase favoring the antiferromagnetic interlayer coupling, whereas the rhombohedral favors ferromagnetic coupling, as observed in experimental studies[18–20] and supported by theoretical calculations.[10,12,13,21] In this study, we investigate the contributions of Cr and I to the interlayer magnetic coupling and the magnetic anisotropy using x-ray spectroscopy measurements on bulk CrI_3 crystals.

The above recent studies have shown a strong tie between interlayer magnetic interaction and structural transition, and thus, we probe the change in the local electronic environment across the transition. x-ray linear dichroism (XLD), the difference between x-ray absorption near edge structure (XANES) spectra obtained with two polarizations, parallel and perpendicular to a crystalline axis, reflects the anisotropy of the electronic states probed in the absorption process. Figure 1(a) shows temperature-dependent XANES at the Cr K edge. The spectra taken with incident polarization parallel to the ab

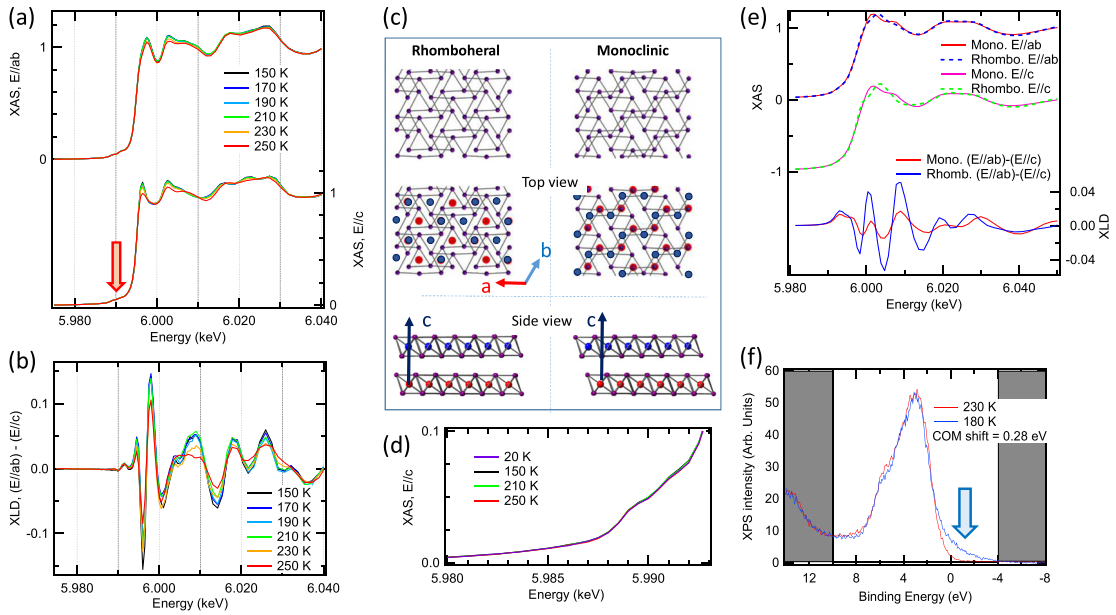

FIG. 1. (a) Temperature dependence of XAS at the Cr K edge. Vertical arrow marks the pre-edge region in the Cr XANES spectra. (b) XLD as a function of temperature. (c) Schematic diagrams of the CrI_3 structure, highlighting edge-sharing octahedra. Purple spheres represent iodine atoms, and Cr (in blue and red) atoms are located at the center of each octahedron. Top schematics show the iodine ions only. Bottom schematics highlight relative Cr orientation between neighboring layers. Note that the layers are shifted fractional lattice coordinates from an ABC stacking, and thus, the Cr ions between the layers are not aligned vertically, whereas it appears so in the side view. (d) Temperature dependence of the pre-edge feature, denoted by the vertical arrow, in (a) is replotted. (e) Simulated Cr K XAS spectra for the high temperature monoclinic and low temperature rhombohedral phases. (f) Temperature-dependent XPS results with the incident photon energy of 750 eV. Below the structural transition, the valence band maximum (VBM) shows an extra spectral weight indicated by the arrow, leading to a center of mass (COM) shift of 0.28 eV. The energy level was calibrated by using the I 5d core levels as reference points. To compensate the temperature-dependent charging effects, the low temperature spectrum was shifted to match the 5d core levels. The effective energy resolution was better than 0.2 eV.

plane (E||ab) and the c-axis (E||c) show noticeable differences. The derived XLD spectra as a function of temperature are shown in Fig. 1(b). The Cr K XANES and XLD exhibit a strong temperature dependence, revealing changes in electronic anisotropy around the Cr atoms. The changes are significant across the known structural transition (210–230 K), whereas minor changes were observable below 210 K. The increased Cr XLD indicates that the electronic environment around the Cr site becomes more anisotropic in the low temperature rhombohedral phase.

To understand the changes in linear dichroism across the monoclinic to rhombohedral structural transition, we carried out simulations of polarization-dependent Cr K-edge XANES using the FEFF8 code.[22] The *ab initio*, self-consistent approach used real space full multiple scattering calculations within an 8 Å cluster centered on the Cr absorbing atom. The cluster was constructed using crystallographic data reported in Ref. 7 for both monoclinic (250 K) and rhombohedral (90 K) phases. The x-ray polarization vector was oriented within or perpendicular to the CrI_3 layers, the former using an average over the in-plane directions. Calculations with linear polarization along the a and b directions show negligible in-plane linear dichroism, in either structure. A Debye model was used to approximate thermal effects on the fine structure although these are, in general, small near absorption threshold. The simulations in Fig. 1(e) show a significant increase in XLD in the low temperature rhombohedral phase, in agreement with experiment. The simulations indicate that changes in c-axis XANES are the main source behind the XLD changes, as expected from a change in layer stacking, which preserves the ab-plane local structure around Cr ions. Despite this agreement, the simulated fine structure does not fully capture the experimental fine structure, suggesting that more complex structural models including potential local structure distortions may be at play. Despite this shortcoming, we note that the predominant structural change across the transition is the shearing of the 2D layers, as illustrated in the bottom schematic in Fig. 1(c), and that this layer stacking change leads to a more anisotropic local environment around the Cr ions.

While the XLD data show an anisotropic electronic environment around Cr, deviation from centrosymmetry in the Cr octahedral environment is insignificant and invariant across the structural transition. The relevant feature in the current Cr XANES data is the pre-edge region, as indicated by a vertical arrow and replotted in Fig. 1(d). The pre-edge structures in transition metal K-edge XANES are linked to the 3d character, via quadrupolar transitions (1s → 3d) or dipole transitions to mixed 3d/4p orbitals. While insignificant in centrosymmetric symmetry, a non-centrosymmetric distortion can enhance the pre-edge features via dipole-allowed transitions.[23–25] The vanishingly small pre-edge intensity in Fig. 1(d), invariant with temperature, indicates the absence of non-centrosymmetric distortion of the CrI_6 octahedra across the monoclinic-to-rhombohedral transition. This result is consistent with x-ray diffraction data.[7] In few-monolayer-thick CrI_3 samples, probing magnetism is nontrivial, and in recent studies, photoluminescence (PL)[26] and second-harmonic generation (SHG)[19] techniques have been used to observe emerging antiferromagnetic

interlayer ordering. These techniques are sensitive to inversion and centrosymmetry breaking, respectively. Our result here shows that the centrosymmetry breaking remains insignificant in both monoclinic and rhombohedral phases, supporting that the origin of the enhanced PL and SHG signals is local spin configuration changes rather than structural ones.

Next, we explored a possible link between the iodine electronic structure across the structural transition. Temperature-dependent changes in I $L_{1,2,3}$ XANES and XLD are shown in Fig. 2. Unlike the strong temperature dependence in the Cr XANES (Fig. 1), the I L XANES spectra show negligible changes between 40 and 220 K. Moreover, while the XLD reveals anisotropies of the probed 5p (I L_1) and 4d, 5s (I $L_{2,3}$) states, there is no clear temperature-dependent changes across the magneto-structural transition. This suggests that changes in the iodine 4d, 5s, and 5p orbital anisotropy across the structural transition are subtle. The schematics in Fig. 1(c), highlighting the iodine ions, provide clues to the negligible change in XLD. The local environment around the iodine ions remains nearly unchanged between the monoclinic and rhombohedral structures, consistent with the insignificant changes in the iodine L-edge XLD.

To further investigate the electronic change across the structural transition, we performed x-ray photoemission spectroscopy (XPS) on CrI_3 crystals. While XANES is sensitive to the unoccupied states, XPS provides valuable insight into the occupied (valence) states. Temperature-dependent XPS spectra below and above the structural transition are shown in Fig. 1(f), revealing a noticeable change in the Cr 3d and I 5p features near the valence band maximum (VBM). Upon cooling from 230 to 180 K, the spectral weight shifts toward lower binding energies, indicating changes in the Cr 3d and I 5p states triggered by the structural transition. Band structure calculations have shown a strong iodine character in the valence band[9,11,27,28] with a strong Cr–I covalency.[17] Combined with the absence of the temperature dependence in the I 5p states in L1 XLD [Fig. 2(c)], the observed weight shift in the XPS spectra suggests potential changes in the Cr 3d features across the structural transition. There is a strong link between the electronic structure near the Fermi level and magnetism, as the p–d covalency and the Cr 3d–I 5p–Cr 3d bond have significant impacts on the anisotropic exchange interactions and consequently on the magnetic anisotropy.[9,15,16] Electronic structure calculations have shown that applied strain or magnetic alignment can have effects on the valence band structure.[27,29,30] Furthermore, recent studies demonstrate the tunability of ferromagnetic and antiferromagnetic ordering in CrI_3 via electrostatic doping.[31–33]

Stemming from strong hybridization between I 5p and Cr 3d, iodine is expected to contribute to magnetism in CrI_3, as shown in theoretical,[9,11–14,21,34] hyperfine field,[35] and iodine $M_{4,5}$ XMCD results.[15] The XMCD data at the Cr $L_{2,3}$ edges reveal no discernable Cr 3d orbital moment contribution,[15,17] and thus, the role of iodine becomes more relevant. In particular, the spin–orbit coupling of the heavy iodine atoms is expected to play a major role in emerging magnetic anisotropy via the anisotropic superexchange[9] and the induced iodine moment is predicted to be −0.12–−0.14 μB/I.[11–13] Along the chromium trihalide series $CrCl_3$, $CrBr_3$, and CrI_3, magnetic anisotropy energy increases, hinting an important role of spin–orbit coupling of the ligands.[36,37] Utilizing the element and orbital selectivity of XMCD technique, we carried out XMCD measurements at the I $L_{1,2,3}$ edges, in order to verify the presence of a significant iodine orbital moment.

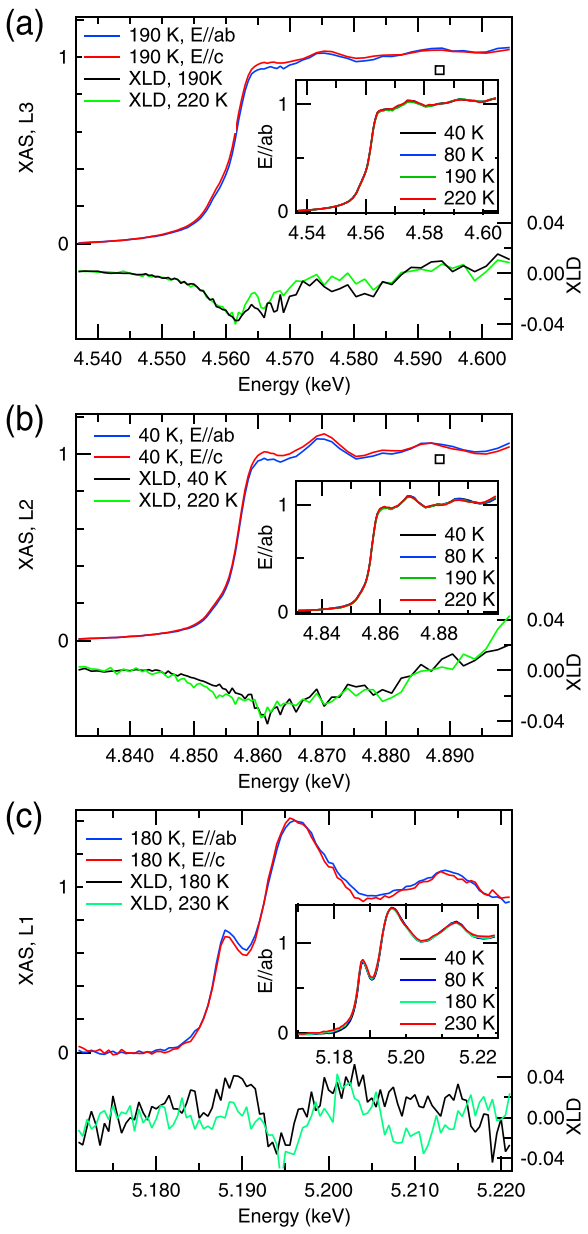

FIG. 2. Temperature and polarization dependence of XAS at the I L_3 (a), L_2 (b), and L_1 (c) edges. The inset in each plot shows that the temperature dependence with the incident polarization parallel to in-plane (E||ab).

The XMCD measurements were conducted on bulk CrI_3 single crystals that are about 8 μm thick along the out-of-plane direction (determined from the x-ray transmission measurement across the I L_1 absorption edge). The XMCD spectra were measured at 10 K, with an applied field of 1 Tesla along the easy axis (c-axis) of the CrI_3 structure [shown in Fig. 1(c)].

Considering the strong hybridization between I 5p and Cr 3d states, we first investigated the iodine orbital moment contribution using I L_1 XMCD since the iodine 5p state is more directly accessible

at the L_1 edge (2s → 5p). While XMCD sum rules[38–40] allow separating orbital ($m_l = -\langle L_z \rangle$) and spin ($m_s = -2\langle S_z \rangle$) magnetic moments, at the K and L_1 absorption edges, due to the absence of spin–orbit split core levels, XMCD sum rules provide orbital moment contribution only.[38,40] At the K and L_1 absorption edges, the integrated XMCD area is proportional to the p state orbital moment, as demonstrated in As K XMCD studies.[41–43] In these studies, a positive XMCD peak corresponds to the p-state orbital moment that is antiparallel to the applied field direction. The XMCD sum rule analysis of I L_1 in Fig. 3(d) gives an iodine 5p orbital moment of −0.018 (±0.004) μB/I. In calculating the orbital moment, we used one hole in the 5p state. This value is an overestimation, considering that the 5p state is full in the nominal electronic configuration of the I^- oxidation state. However, as revealed in the density of state calculation studies, the 5p states in CrI_3 remain less than full.[9–13,33,44] The orbital moment from the XMCD sum rules is simply proportional to the number of 5p holes, and the result can be considered as an upper limit estimate for the iodine 5p orbital moment. The negative sign of the orbital moment here indicates that the iodine 5p orbital moment is antiparallel to the applied field direction and, thus, antiparallel to the dominant Cr 3d spin moment. This resembles the antiparallel alignment between the Mn 3d spin and As 5p orbital moments in MnAs- and $Ba_2Mn_2As_2$-based alloys.[41,43]

Figures 3(a) and 3(b) show sizable XMCD signals at the I $L_{2,3}$ edge, corresponding to the 2p → 4d,5s transitions. The field dependence of the I L_2 XMCD in the inset in Fig. 3(b) shows that the signal is saturated well below an applied field of 1 Tesla and is overall consistent with the magnetometry result from bulk CrI_3.[7] The iodine 4d states are nominally full, as evidenced by a negligible XAS peak (white line) near the I $L_{2,3}$ absorption threshold energy. Thus, transitions into states with pure 4d character are unlikely, and it is plausible that the probed state includes the iodine 5s state, which is hybridized with the iodine 5p state. This scenario is supported by the observed iodine magnetic hyperfine signature, originating from the hybridized iodine 5s-5p orbitals, in Mossbauer measurements,[35] and in the presence of Cr(3d)-I(5s5p) hybridization in a theoretical study.[44] Due to uncertainties in the number of I 5s and 4d holes and negligible white-line features in XAS, isolating orbital and spin moment via XMCD sum rules[38–40] is not straightforward. Instead, we focus on the ratio between orbital and spin moments, which is independent of these factors. The corresponding orbital to spin ratio from the I $L_{2,3}$ XMCD data is estimated to be 6.5 (±0.3)%, and the result reveals that the iodine orbital moment is small relative to its spin counterpart. The overall I L XMCD results show clear evidence for induced iodine magnetic moment and, in particular, for iodine 5p orbital moment. Given the hybridized and extended nature of the iodine 5p ligands in CrI_3, the iodine orbital moment may be involved in mediating anisotropic exchange for incipient magnetic anisotropy.

In summary, element-specific x-ray measurements revealed a measurable orbital moment at the iodine sites, as well as changes in the anisotropy of the Cr local environment across the structural transition. Moreover, below the structural transition temperature, the observed anisotropy increase is accompanied by a XPS spectral weight shift, alluding to potential changes in the Cr 3d states. As shown in the doped tetradymite chalcogenides[45] and dilute magnetic semiconductors,[46] modification in the 3d density of states near the Fermi level can have a significant impact on the p-d exchange magnetic interactions.

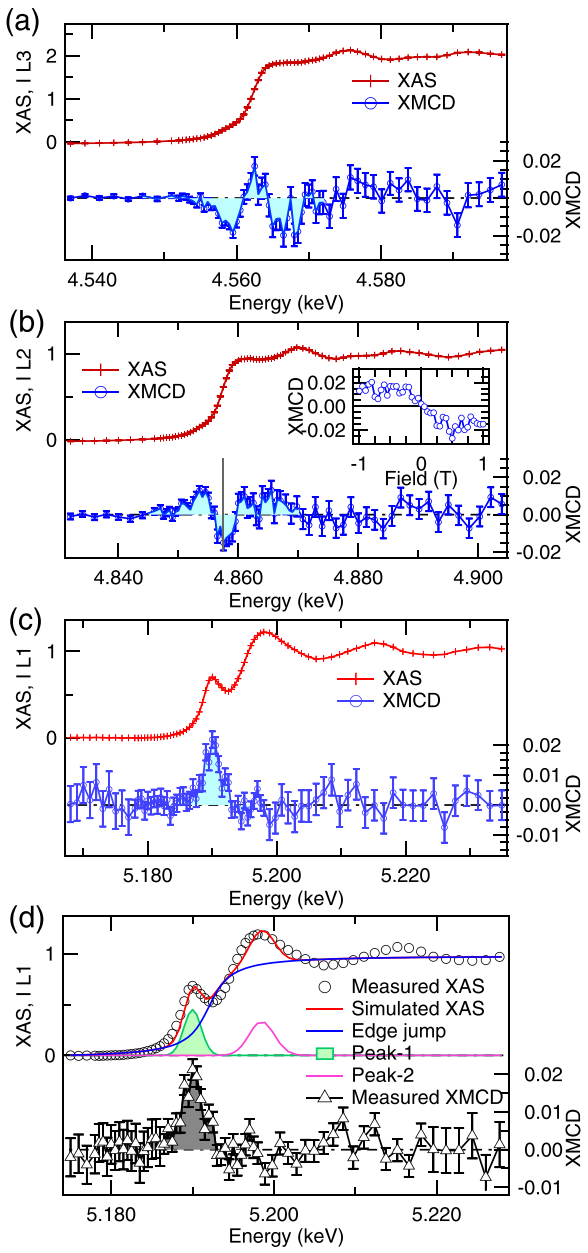

FIG. 3. XMCD at the I $L_{3,2,1}$ edges at 10 K, with an external field of 1 Tesla along the c-axis of CrI_3. (a) Iodine L_3 XMCD, (b) L_2 XMCD, and (c) L_1 XMCD. The shaded areas in the XMCD spectra indicate the ranges used for XMCD sum rules. The inset in (b) shows the field dependence of the L_2 XMCD at the incident energy (4.857 keV) indicated by the vertical line. (d) Simulated edge jump and peaks used in the I L_1 XMCD sum rule analysis.

Our results highlight the electronic environment changes across the structural transition, which may be linked to the incipient magnetic ordering and anisotropy in the low temperature phase. Our iodine XMCD result provides direct evidence for small iodine 5p orbital moment, alternatively suggesting the prominence of the anisotropic

superexchange interaction as the main source of the magnetic anisotropy in CrI_3, as predicted from the theoretical studies.[9,15,16]

X-ray absorption and photoemission experiments were carried out at beamlines 4-ID-D, 6-ID-B, and 29-ID of the Advanced Photon Source, Argonne National Laboratory. The work performed at the Advanced Photon Source was supported by the U.S. Department of Energy, Office of Science, and Office of Basic Energy Sciences under Contract No. DE-AC02-06CH11357. Crystal growth and characterization at ORNL were supported by the U. S. Department of Energy, Office of Science, Basic Energy Sciences, Materials Sciences and Engineering Division under Contract No. DE-AC05-00OR22725.

DATA AVAILABILITY

The data that support the findings of this study are available from the corresponding author upon reasonable request.

REFERENCES

[1]T. Song, X. Cai, M. W.-Y. Tu, X. Zhang, B. Huang, N. P. Wilson, K. L. Seyler, L. Zhu, T. Taniguchi, K. Watanabe, M. A. McGuire, D. H. Cobden, D. Xiao, W. Yao, and X. Xu, Science **360**, 1214 (2018).
[2]D. R. Klein, D. MacNeill, J. L. Lado, D. Soriano, E. Navarro-Moratalla, K. Watanabe, T. Taniguchi, S. Manni, P. Canfield, J. Fernández-Rossier, and P. Jarillo-Herrero, Science **360**, 1218 (2018).
[3]Z. Wang, I. Gutiérrez-Lezama, N. Ubrig, M. Kroner, M. Gibertini, T. Taniguchi, K. Watanabe, A. Imamoğlu, E. Giannini, and A. F. Morpurgo, Nat. Commun. **9**, 2516 (2018).
[4]H. H. Kim, B. Yang, T. Patel, F. Sfigakis, C. Li, S. Tian, H. Lei, and A. W. Tsen, Nano Lett. **18**, 4885 (2018).
[5]N. D. Mermin and H. Wagner, Phys. Rev. Lett. **17**, 1133 (1966).
[6]B. Huang, G. Clark, E. Navarro-Moratalla, D. R. Klein, R. Cheng, K. L. Seyler, D. Zhong, E. Schmidgall, M. A. McGuire, D. H. Cobden, W. Yao, D. Xiao, P. Jarillo-Herrero, and X. Xu, Nature **546**, 270 (2017).
[7]M. A. McGuire, H. Dixit, V. R. Cooper, and B. C. Sales, Chem. Mater. **27**, 612 (2015).
[8]W.-B. Zhang, Q. Qu, P. Zhu, and C.-H. Lam, J. Mater. Chem. C **3**, 12457 (2015).
[9]J. L. Lado and J. Fernández-Rossier, 2D Mater. **4**, 035002 (2017).
[10]N. Sivadas, S. Okamoto, X. Xu, C. J. Fennie, and D. Xiao, Nano Lett. **18**, 7658 (2018).
[11]O. Besbes, S. Nikolaev, N. Meskini, and I. Solovyev, Phys. Rev. B **99**, 104432 (2019).
[12]S. W. Jang, M. Y. Jeong, H. Yoon, S. Ryee, and M. J. Han, Phys. Rev. Mater. **3**, 031001 (2019).
[13]P. Jiang, C. Wang, D. Chen, Z. Zhong, Z. Yuan, Z.-Y. Lu, and W. Ji, Phys. Rev. B **99**, 144401 (2019).
[14]B. Yang, X. Zhang, H. Yang, X. Han, and Y. Yan, J. Phys. Chem. C **123**, 691 (2019).
[15]D.-H. Kim, K. Kim, K.-T. Ko, J. Seo, J. S. Kim, T.-H. Jang, Y. Kim, J.-Y. Kim, S.-W. Cheong, and J.-H. Park, Phys. Rev. Lett. **122**, 207201 (2019).
[16]I. Lee, F. G. Utermohlen, D. Weber, K. Hwang, C. Zhang, J. van Tol, J. E. Goldberger, N. Trivedi, and P. C. Hammel, Phys. Rev. Lett. **124**, 017201 (2020).
[17]A. Frisk, L. B. Duffy, S. Zhang, G. van der Laan, and T. Hesjedal, Mater. Lett. **232**, 5 (2018).
[18]L. Thiel, Z. Wang, M. A. Tschudin, D. Rohner, I. Gutiérrez-Lezama, N. Ubrig, M. Gibertini, E. Giannini, A. F. Morpurgo, and P. Maletinsky, Science **364**, 973 (2019).
[19]Z. Sun, Y. Yi, T. Song, G. Clark, B. Huang, Y. Shan, S. Wu, D. Huang, C. Gao, Z. Chen, M. McGuire, T. Cao, D. Xiao, W.-T. Liu, W. Yao, X. Xu, and S. Wu, Nature **572**, 497 (2019).
[20]B. Niu, T. Su, B. A. Francisco, S. Ghosh, F. Kargar, X. Huang, M. Lohmann, J. Li, Y. Xu, T. Taniguchi, K. Watanabe, D. Wu, A. Balandin, J. Shi, and Y.-T. Cui, Nano Lett. **20**, 553 (2020).
[21]D. Soriano, C. Cardoso, and J. Fernández-Rossier, Solid State Commun. **299**, 113662 (2019).
[22]A. L. Ankudinov, B. Ravel, J. J. Rehr, and S. D. Conradson, Phys. Rev. B **58**, 7565 (1998).
[23]J. E. Hahn, R. A. Scott, and E. I. Solomon, Chem. Phys. Lett. **88**, 595 (1982).
[24]J. C. Woicik, E. L. Shirley, C. S. Hellberg, K. E. Andersen, S. Sambasivan, D. A. Fischer, B. D. Chapman, E. A. Stern, P. Ryan, D. L. Ederer, and H. Li, Phys. Rev. B **75**, 140103 (2007).
[25]E. A. Stern, Phys. Rev. Lett. **93**, 037601 (2004).
[26]K. L. Seyler, D. Zhong, D. R. Klein, S. Gao, X. Zhang, B. Huang, E. Navarro-Moratalla, L. Yang, D. H. Cobden, M. A. McGuire, W. Yao, D. Xiao, P. Jarillo-Herrero, and X. Xu, Nat. Phys **14**, 277 (2018).
[27]Z. Wu, J. Yu, and S. Yuan, Phys. Chem. Chem. Phys. **21**, 7750 (2019).
[28]H. Wang, V. Eyert, and U. Schwingenschlögl, J. Phys.: Condens. Matter **23**, 116003 (2011).
[29]L. Webster and J.-A. Yan, Phys. Rev. B **98**, 144411 (2018).
[30]P. Jiang, L. Li, Z. Liao, Y. X. Zhao, and Z. Zhong, Nano Lett. **18**, 3844 (2018).
[31]S. Jiang, L. Li, Z. Wang, K. F. Mak, and J. Shan, Nat. Nanotechnol. **13**, 549 (2018).
[32]S. Jiang, J. Shan, and K. F. Mak, Nat. Mater. **17**, 406 (2018).
[33]J. Kim, K.-W. Kim, B. Kim, C.-J. Kang, D. Shin, S.-H. Lee, B.-C. Min, and N. Park, Nano Lett. **20**, 929 (2020).
[34]B. Yang, X. Zhang, H. Yang, X. Han, and Y. Yan, Appl. Phys. Lett. **114**, 192405 (2019).
[35]J. P. Sanchez, B. Djermouni, J. M. Friedt, and G. K. Shenoy, Hyperfine Interact. **1**, 313 (1975).
[36]N. Richter, D. Weber, F. Martin, N. Singh, U. Schwingenschlögl, B. V. Lotsch, and M. Kläui, Phys. Rev. Mater. **2**, 024004 (2018).
[37]M. A. McGuire, G. Clark, S. Kc, W. M. Chance, G. E. Jellison, V. R. Cooper, X. Xu, and B. C. Sales, Phys. Rev. Mater. **1**, 014001 (2017).
[38]P. Carra, B. T. Thole, M. Altarelli, and X. Wang, Phys. Rev. Lett. **70**, 694 (1993).
[39]C. T. Chen, Y. U. Idzerda, H.-J. Lin, N. V. Smith, G. Meigs, E. Chaban, G. H. Ho, E. Pellegrin, and F. Sette, Phys. Rev. Lett. **75**, 152 (1995).
[40]B. T. Thole, P. Carra, F. Sette, and G. van der Laan, Phys. Rev. Lett. **68**, 1943 (1992).
[41]P. Wadley, A. A. Freeman, K. W. Edmonds, G. van der Laan, J. S. Chauhan, R. P. Campion, A. W. Rushforth, B. L. Gallagher, C. T. Foxon, F. Wilhelm, A. G. Smekhova, and A. Rogalev, Phys. Rev. B **81**, 235208 (2010).
[42]B. G. Ueland, A. Pandey, Y. Lee, A. Sapkota, Y. Choi, D. Haskel, R. A. Rosenberg, J. C. Lang, B. N. Harmon, D. C. Johnston, A. Kreyssig, and A. I. Goldman, Phys. Rev. Lett. **114**, 217001 (2015).
[43]F. Sun, G. Q. Zhao, C. A. Escanhoela, B. J. Chen, R. H. Kou, Y. G. Wang, Y. M. Xiao, P. Chow, H. K. Mao, D. Haskel, W. G. Yang, and C. Q. Jin, Phys. Rev. B **95**, 094412 (2017).
[44]I. V. Kashin, V. V. Mazurenko, M. I. Katsnelson, and A. N. Rudenko, 2D Mater. **7**, 025036 (2020).
[45]M. G. Vergniory, M. M. Otrokov, D. Thonig, M. Hoffmann, I. V. Maznichenko, M. Geilhufe, X. Zubizarreta, S. Ostanin, A. Marmodoro, J. Henk, W. Hergert, I. Mertig, E. V. Chulkov, and A. Ernst, Phys. Rev. B **89**, 165202 (2014).
[46]K. Sato, L. Bergqvist, J. Kudrnovský, P. H. Dederichs, O. Eriksson, I. Turek, B. Sanyal, G. Bouzerar, H. Katayama-Yoshida, V. A. Dinh, T. Fukushima, H. Kizaki, and R. Zeller, Rev. Mod. Phys. **82**, 1633 (2010).